A Procedure to Infer Lightning Return-Stroke Current Waveform From Far-Field Waveform for the Case of Lossy Ground

Shunsuke Koike, Masahiro Fukuyama, Yoshihiro Baba, *Fellow, IEEE*, Toshihiro Tsuboi, and Vladimir A. Rakov, *Fellow, IEEE*

***Abstract*—We proposed expressions for reconstructing the waveform of channel-base current from the corresponding far electric field waveform (radiation field component only) on perfectly conducting ground for the modified transmission line models with linear and exponential current decay with height. Waveforms of vertical electric field on lossy ground at far distances (50–200 km) were computed using the finite-difference time-domain (FDTD) method for solving discretized Maxwell's equations in the 2-D cylindrical coordinate system. The FDTD-computed waveforms of vertical electric field on lossy ground were compensated for propagation effects and used in the proposed field-to-current conversion expressions for inferring the channel-base current waveform. The reconstructed currents are in excellent agreement with the current used in computing the fields on lossy ground.**

***Index Terms*—Finite-difference time-domain (FDTD) method, lightning, propagation effects, return-stroke current waveform, return-stroke field waveform, return-stroke model.**

I. Introduction

IT is of practical interest to infer lightning parameters, including return-stroke current waveform, from measured far electric or magnetic fields (e.g., Rakov [1], Section 4.5.6).

Popov et al. [2] have proposed two procedures to infer both the parameters of the DU model (the discharge time constant, the return-stroke speed, and downward-current propagation speed) and the channel-base current from fields on perfectly conducting ground at two different distances: (i) E_z or azimuthal magnetic field B_ϕ at far and near distances or (ii) B_ϕ at intermediate and near distances. An explicit inversion formula using both the induction and radiation terms of B_ϕ was derived for (ii) and the genetic algorithm was used. However, lossy ground effects were not taken into account.

Manuscript received 7 December 2022; revised 18 May 2023; accepted 14 October 2023. This work was supported by the U.S. National Science Foundation under Grant AGS-2055178. *(Corresponding author: Yoshihiro Baba.)*

Shunsuke Koike, Masahiro Fukuyama, and Yoshihiro Baba are with the Doshisha University, Kyoto 610-0394, Japan (e-mail: ctwg0314@mail4.doshisha.ac.jp; hiro.den.east@gmail.com; ybaba@mail.doshisha.ac.jp).

Toshihiro Tsuboi is with the TEPCO Research Institute, Kanagawa 230-0002, Japan (e-mail: tsuboi.toshihiro@tepco.co.jp).

Vladimir A. Rakov is with the Department of Electrical and Computer Engineering, University of Florida, Gainesville, FL 32611 USA (e-mail: rakov@ece.ufl.edu).

Digital Object Identifier 10.1109/TEMC.2023.3325280

In this article, recurrence expressions for inferring the channel-base current from the waveform of far vertical electric field on perfectly conducting ground are proposed for the modified transmission line model with linear current decay with height (MTLL) [3] and the modified transmission line model with exponential current decay with height (MTLE) [4]. Furthermore, field waveforms degraded by propagation effects are computed using the finite-difference time-domain (FDTD) method [5] for solving discretized Maxwell's equations in the 2-D cylindrical coordinate system and then compensated for propagation effects using a procedure in the frequency domain proposed by Cooray [6]. Finally, the proposed field-to-current conversion expressions are used for inferring the channel-base current waveform from the waveforms of vertical electric field compensated, using the proposed recurrence expressions, for propagation effects. Thus, the procedure to infer the channel-base current waveform from the far-field waveform for the case of lossy ground is composed of two steps: the first step is to compensate the far-field waveform degraded due to propagation over lossy ground, and the second step is to reconstruct the channel-base current waveform from the compensated far-field waveform. This article is based on conference presentation by Fukuyama et al. [7].

II. Field-to-Current Conversion Expressions for MTLL and MTLE Models

The conversion expressions will be derived for the radiation field component only that is expected to be dominant at distances $\geq$ 50 km (see, for example, Fig. 4.32 of [1]).

A. MTLL Model

For a vertical lightning channel over perfectly conducting ground, the radiation component of vertical electric field E_z at horizontal distance r at time t is approximately given as follows:

$$E_z(r,t) \approx -\frac{1}{2\pi\varepsilon_0 c^2 r}\int_0^{L(t)} \frac{\partial I(z', t-r/c)}{\partial t}\,\mathrm{d}z' \quad (1)$$

where ε_0 is the permittivity of free space, c is the speed of light, $I(z',t)$ is the current at height z' at time t, and $L(t)$ is the radiating channel length that is given by $L(t) = v\cdot(t\text{-}r/c)vt$ - r/c, where v is the return-stroke current wave propagation speed along the channel.

In the MTLL model [3], the relation between the current at height z' and at the channel base, $z' = 0$, is as follows:

$$I(z',t) = (1 - z'/H)\, I(0, t - z'/v) \tag{2}$$

where H is the total channel length. In this model, current wave propagates upward along the lightning channel at speed v with linear attenuation, and it is zero at height $z' = H$.

Substituting (2) into (1) yields

$$\begin{aligned}
&E_z(r,t) \\
&\approx -\frac{1}{2\pi\varepsilon_0 c^2 r}\int_0^{L(t)} \frac{\partial I(z', t - r/c)}{\partial t}\,\mathrm{d}z' \\
&= -\frac{1}{2\pi\varepsilon_0 c^2 r}\int_0^{L(t)} (-v)\,\frac{\partial}{\partial z'} \\
&\quad \left[\left(1 - \frac{z'}{H}\right) I\left(0, t - \frac{z'}{v} - \frac{r}{c}\right)\right]\mathrm{d}z' \\
&= \frac{v}{2\pi\varepsilon_0 c^2 r}\left[(1 - z'/H)\, I(0, t - z'/v - r/c)\right] \Big|_0^{L(t)} \\
&\quad - \frac{v}{2\pi\varepsilon_0 c^2 r}\int_0^{L(t)} \left(-\frac{1}{H}\right) I(0, t - z'/v - r/c)\,\mathrm{d}z' \\
&= \frac{v}{2\pi\varepsilon_0 c^2 r}\left[\begin{array}{l} (1 - L(t)/H)\, I(0,0) \\ -(1 - 0/H)\, I(0, t - 0/v - r/c) \end{array}\right] \\
&\quad + \frac{v}{2\pi\varepsilon_0 c^2 r}\frac{1}{H}\int_0^{L(t)} I(0, t - z'/v - r/c)\,\mathrm{d}z' \\
&= \frac{v}{2\pi\varepsilon_0 c^2 r}\left[0 - I(0, t - r/c)\right] \\
&\quad + \frac{v}{2\pi\varepsilon_0 c^2 r}\frac{1}{H}\int_0^{L(t)} I(0, t - z'/v - r/c)\;\mathrm{d}z' \\
&= -\frac{v}{2\pi\varepsilon_0 c^2 r} I(0, t - r/c) \\
&\quad + \frac{v}{2\pi\varepsilon_0 c^2 r}\frac{1}{H}\int_0^{L(t)} I(0, t - z'/v - r/c)\;\mathrm{d}z'.
\end{aligned} \tag{3}$$

Approximating the integral in (3) by summation yields

$$\begin{aligned}
E_z(n\Delta t + r/c) \approx &-\frac{v}{2\pi\varepsilon_0 c^2 r} I(n\Delta t) \\
&+\frac{v}{2\pi\varepsilon_0 c^2 r}\frac{1}{H}\sum_{k=1}^{m-1} I(n\Delta t - k\Delta t)\cdot v\Delta t
\end{aligned} \tag{4}$$

where $m = n$ for $n \le H/(v\Delta t)$ and $m = H/(v\Delta t)$ for $n > H/(v\Delta t)$. Note that in (4) $E_z(r,t)$ and $I(0,t)$ are abbreviated as $E_z(t)$ and $I(t)$, respectively, and that the time reference is placed at the channel base.

From (4), the channel-base current is expressed as follows:

$$\begin{aligned}
I(n\Delta t) = &-\frac{2\pi\varepsilon_0 c^2 r}{v} E_z(n\Delta t + r/c) \\
&+ \frac{v\Delta t}{H}\sum_{k=1}^{m-1} I(n\Delta t - k\Delta t).
\end{aligned} \tag{5}$$

B. MTLE Model

In the MTLE model [4], the relation between the current at height z' and at the channel base is as follows:

$$I(z',t) = \exp(-z'/\lambda)\, I(0, t - z'/v) \tag{6}$$

where λ is the current decay height constant. In this model, current wave propagates upward at speed v with exponential attenuation. The magnitude of current at $z' = 7$ km is 3 % of that at the channel base for often assumed $\lambda = 2$ km, which corresponds to 0.3 kA for 10 kA at the channel base. In this study, we set H to 7 km and v to $0.5c$ and show the computed field waveforms up to 45 μs, so that they are not influenced by the effect of this residual current at the top of the channel.

Substituting (6) into (1) yields

$$\begin{aligned}
&E_z(r,t) \approx \\
&-\frac{1}{2\pi\varepsilon_0 c^2 r}\int_0^{L(t)} \frac{\partial}{\partial t}\left[\exp\left(-\frac{z'}{\lambda}\right) I\left(0, t - \frac{z'}{v} - \frac{r}{c}\right)\right]\mathrm{d}z' \\
&= -\frac{1}{2\pi\varepsilon_0 c^2 r}\int_0^{L(t)} (-v)\,\frac{\partial}{\partial z'} \\
&\quad \left[\exp\left(-\frac{z'}{\lambda}\right) I\left(0, t - \frac{z'}{v} - \frac{r}{c}\right)\right]\mathrm{d}z' \\
&= \frac{v}{2\pi\varepsilon_0 c^2 r}\left[\exp\left(-\frac{z'}{\lambda}\right) I(0, t - z'/v - r/c)\right] \Big|_0^{L(t)} \\
&\quad - \frac{v}{2\pi\varepsilon_0 c^2 r}\int_0^{L(t)} \left(-\frac{1}{\lambda}\right)\exp\left(-\frac{z'}{\lambda}\right) \\
&\quad I(0, t - z'/v - r/c)\;\mathrm{d}z' \\
&= \frac{v}{2\pi\varepsilon_0 c^2 r}\left[\begin{array}{l} \exp\left(-\frac{L(t)}{\lambda}\right) I(0,0) \\ -\exp\left(-\frac{0}{\lambda}\right) I(0, t - 0/v - r/c) \end{array}\right] \\
&\quad + \frac{v}{2\pi\varepsilon_0 c^2 r}\frac{1}{\lambda}\int_0^{L(t)} \exp\left(-\frac{z'}{\lambda}\right) I(0, t - z'/v - r/c)\,\mathrm{d}z' \\
&= \frac{v}{2\pi\varepsilon_0 c^2 r}\left[0 - I(0, t - r/c)\right] \\
&\quad + \frac{v}{2\pi\varepsilon_0 c^2 r}\frac{1}{\lambda}\int_0^{L(t)} \exp\left(-\frac{z'}{\lambda}\right) I(0, t - z'/v - r/c)\;\mathrm{d}z' \\
&= -\frac{v}{2\pi\varepsilon_0 c^2 r} I(0, t - r/c) \\
&\quad + \frac{v}{2\pi\varepsilon_0 c^2 r}\frac{1}{\lambda}\int_0^{L(t)} \exp\left(-\frac{z'}{\lambda}\right) I(0, t - z'/v - r/c)\;\mathrm{d}z'.
\end{aligned} \tag{7}$$

Approximating the integral in (7) by summation yields

$$\begin{aligned}
E_z(n\Delta t + r/c) \approx &-\frac{v}{2\pi\varepsilon_0 c^2 r} I(n\Delta t) \\
&+\frac{v}{2\pi\varepsilon_0 c^2 r}\frac{1}{\lambda}\sum_{k=1}^{m-1} \exp\left(-\frac{k\, v\Delta t}{\lambda}\right) I(n\Delta t - k\Delta t)\cdot v\Delta t
\end{aligned} \tag{8}$$

where m and n are defined in the same way as in (4). In fact, the only difference between (8) and (4) is in the second term: $1/\lambda$ and $\exp(-k\,v\Delta t/\lambda)$ in (8) versus $1/H$ in (4).

From (8), the channel-base current is expressed as follows:

$$I(n\Delta t) = -\frac{2\pi\varepsilon_0 c^2 r}{v} E_z(n\Delta t + r/c) + \frac{v\Delta t}{\lambda}\sum_{k=1}^{m-1}\exp(-k\,v\Delta t/\lambda)\,I(n\Delta t - k\Delta t). \tag{9}$$

Note that, for the MTLE model, Rachidi and Thottappillil [8] derived the relation between $dI(0, t)/dt$ and far electric field $E_z(r, t + r/c)$ and its time derivative $dE_z(r, t + r/c)/dt$. Equation (9) is simpler and easier to use than theirs.

III. Compensation of Field Propagation Effects

In the case of finite ground conductivity, the peak of far electromagnetic field decreases and the risetime increases due to preferential attenuation of higher frequency components relative to that on perfectly conducting ground. In [6], it is shown that the radiation component of vertical electric field of angular frequency ω at distance r on the ground having conductivity σ, $E_z(r, j\omega, \sigma)$, can be approximately estimated from the corresponding vertical electric field on perfectly conducting ground, $E_z(r, j\omega, \sigma = \infty)$. Therefore, $E_z(r, j\omega, \sigma = \infty)$ can be recovered from $E_z(r, j\omega, \sigma)$; that is, fields on lossy ground can be compensated for propagation effects. The procedure is given as follows:

$$\begin{cases} E_z(r, j\omega, \sigma = \infty) = \frac{E_z(r, j\omega, \sigma)}{F(r, j\omega, \sigma)} \\ F(r, j\omega, \sigma) = 1 - j\sqrt{\pi p}\exp(-p)\,erfc\left(j\sqrt{p}\right) \\ p = -\frac{1}{2}j\omega\sqrt{\varepsilon_0\mu_0}\,r\Delta^2 \\ \Delta = \sqrt{\frac{\varepsilon_0}{\mu_0}}\,\frac{\sqrt{j\omega\mu_0(\sigma + j\omega\varepsilon_r\varepsilon_0) + \omega^2\varepsilon_0\mu_0}}{\sigma + j\omega\varepsilon_r\varepsilon_0} \end{cases} \tag{10}$$

where F is the attenuation function, $erfc$ is the error function, μ_0 is the permeability of free space, and ε_r is the relative permittivity of ground.

IV. FDTD Calculations of Far Fields on Perfectly Conducting Ground

Fig. 1 shows the model to be used in simulations with the FDTD method in the 2-D cylindrical coordinate system. The computational domain is 250 km × 100 km, which is divided uniformly into rectangular cells of 3 m × 3 m. The time increment is set to 7.01 ns. Liao's second-order absorbing boundary condition [9] is applied to the perimeter of the computational domain except for its left-side edge. The thickness of ground is set to 1 km. The ground conductivity σ is set to 0.1, 1, 10, 100 mS/m, or ∞. The vertical lightning return-stroke channel, which is represented by the phased-current source array [10], is placed at the left-side boundary. The waveform of channel-base current is represented by the Heidler function [11], as an example, and is given as follows:

$$I(0, t) = \frac{I_{01}}{\eta}\frac{(t/\tau_1)^2}{1 + (t/\tau_1)^2}e^{-t/\tau_2}. \tag{11}$$

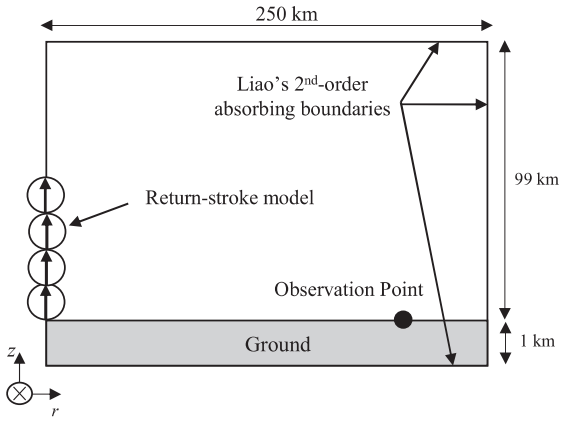

Fig. 1. Configuration used in simulations with the FDTD method in the 2-D cylindrical coordinate system.

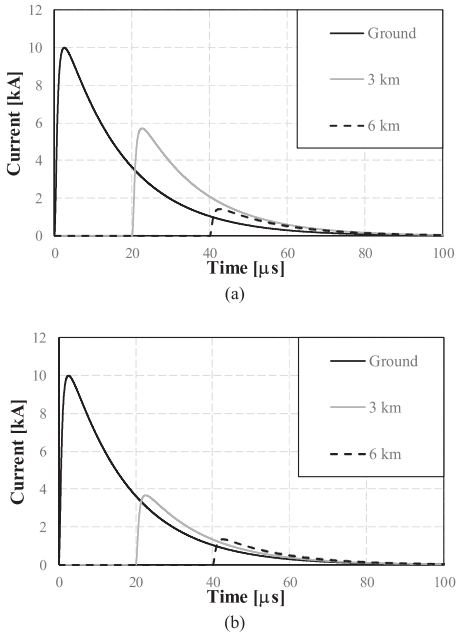

Fig. 2. Waveforms of lightning return-stroke current at heights $z' = 0$ (ground), 3, and 6 km for (a) MTLL model with $H = 7$ km and (b) MTLE model with $\lambda = 2$ km. The current-wave propagation speed $v = 0.5c$ for both models.

Fig. 2(a) and (b) show waveforms of current at heights $z' = 0$, 3, and 6 km for the MTLL model with $H = 7$ km and the MTLE model with $\lambda = 2$ km, respectively. The current-propagation speed v is set to 0.5 c, and the length of the lightning channel is set to 7 km for both models. The peak value of the channel-base current is 10 kA, and the risetime is 1 μs, for which the parameters of (11) are set as follows: $I_{01} = 10$ kA, $\eta = 0.785$, $\tau_1 = 0.75$ μs, and $\tau_2 = 16$ μs. Simulations were also carried out for the channel-base current with a magnitude of 10 kA and a risetime of 5 μs, for which the parameters were set as follows: $I_{01} = 10$ kA, $\eta = 0.592$, $\tau_1 = 2.45$ μs, and $\tau_2 = 16$ μs, although the current waveforms are not shown here.

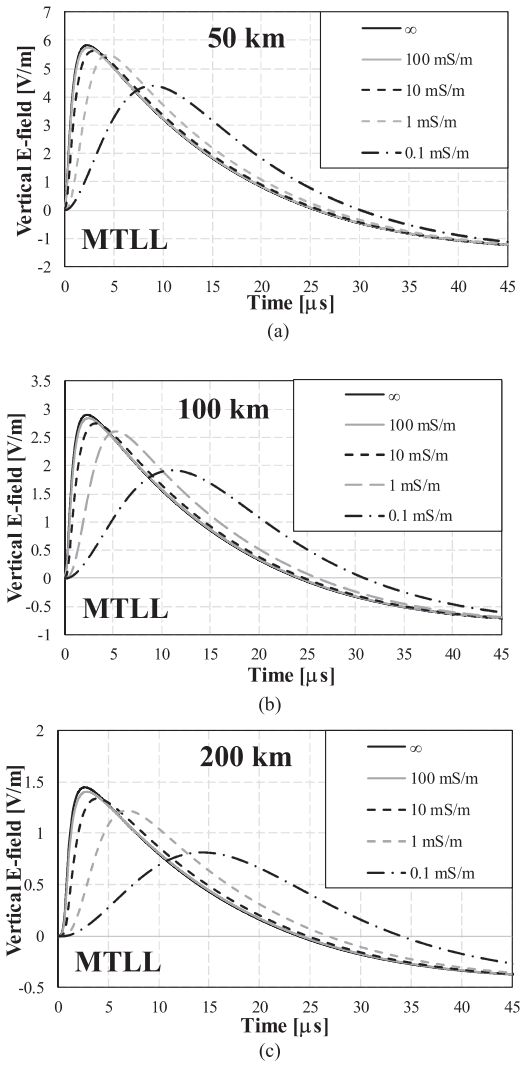

Fig. 3. Waveforms of vertical electric field E_z at distances of (a) $r = 50$ km, (b) $r = 100$ km, and (c) $r = 200$ km from the lightning channel, computed using the FDTD method and the MTLL model for different values of ground conductivity: $\sigma = 0.1$, 1, 10, 100 mS/m, and ∞. Lightning current risetime RT is 1 μs.

V. Analysis and Discussion

A. FDTD-computed E_z Waveforms Degraded by Propagation Effects

Fig. 3(a)–(c) show waveforms of vertical electric field E_z at distances of 50, 100, and 200 km, respectively, from the lightning channel, computed using the FDTD method with the MTLL model for the current risetime $RT = 1$ μs and for different values of ground conductivity: $\sigma = 0.1$, 1, 10, 100 mS/m, and ∞ (perfect ground). Fig. 4(a) and (b) show those at 50 and 200 km, respectively, for $RT = 5$ μs. Fig. 5 is the same as Fig. 3, but for the MTLE model. Note that the FDTD-computed fields are total fields (include all three field components, but at the distances of interest (50–200 km) they are dominated by the radiation component.

It appears from Figs. 3–5 that waveforms of E_z for $\sigma = 100$ mS/m (and higher) are almost identical to those for $\sigma = \infty$.

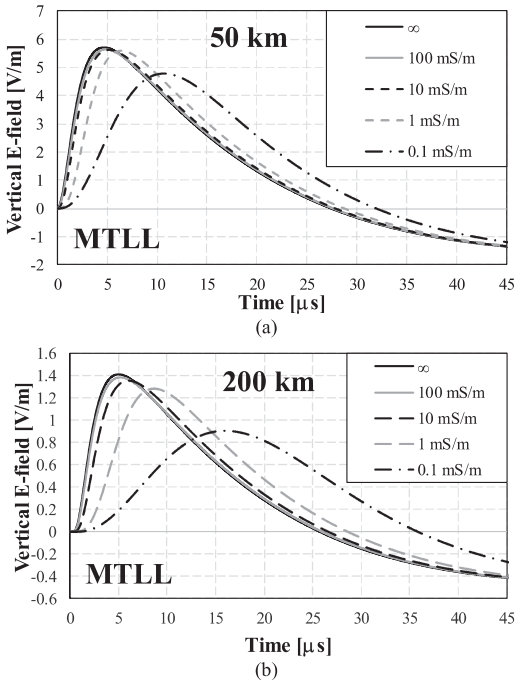

Fig. 4. Same as Fig. 3(a) and (c), but for $RT = 5$ μs.

With decreasing σ , the attenuation and distortion of E_z become more significant. Specifically, the field peak decreases, while both the risetime and zero-crossing time increase, as expected.

B. E_z Waveforms Compensated for Propagation Effects

Figs. 6–8 show waveforms of E_z at distances of 50 and 200km compensated for propagation effects using (10). Note that the upper frequency bound in using (10) was determined by the time increment employed in the FDTD calculations presented in Section IV, and the frequency increment was determined by the time window or the maximum observation time. As a result of compensation, effects of propagation over lossy ground are removed, so that the compensated fields should correspond to those on perfectly conducting ground. It appears from Figs. 6–8 that the FDTD-computed waveforms of E_z on ground with σ ranging from 100 S/m to 0.1 mS/m after compensation become indistinguishable from or very close to those calculated for $\sigma = \infty$. Thus, the procedure proposed in [6] and outlined in Section III works very well under the conditions considered in this study.

C. Channel-Base Current Waveforms Reconstructed From Compensated E_z Waveforms

Fig. 9 shows waveforms of lightning current at the channel base reconstructed from compensated electric-field waveforms, computed using the MTLL model for $RT = 1$ μs and shown in Fig. 6. Reconstruction was done using (5).

Similarly, Fig. 10 shows waveforms of lightning current at the channel base reconstructed from compensated electric-field waveforms, computed using the MTLE model for $RT = 1$ μs and shown in Fig. 8. Reconstruction was done using (9).

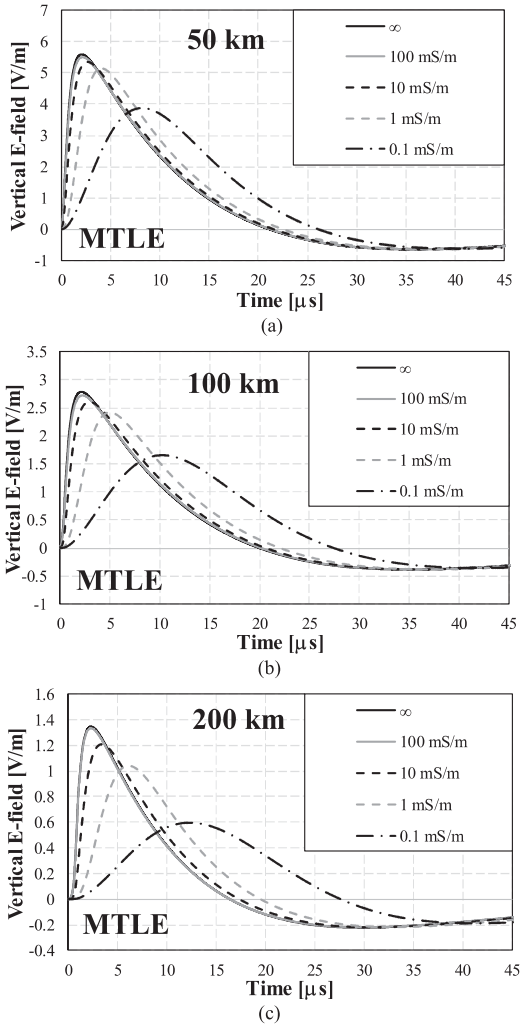

Fig. 5. Same as Fig. 3, but for the MTLE model.

TABLE I
PEAK VALUES OF ESTIMATED CHANNEL-BASE CURRENT IN KA FOR THE MTLL MODEL AND $RT = 1$ μS

Distance	Ground conductivity σ, mS/m			
r, km	0.1	1	10	100
50	9.89	9.92	9.95	9.98
100	9.86	9.89	9.95	9.98
200	9.78	9.88	9.94	9.97

Tables I and II give peak values of reconstructed channel-base current for the MTLL model and $RT = 1$ and 5 μs, respectively. Tables III and IV are the same as Tables I and II, respectively, but for the MTLE model.

It appears from Figs. 9 and 10 that channel-base current waveforms can be reasonably well reconstructed from E_z waveforms degraded by propagation effects using the proposed two-step procedure. Also, it follows from Tables I–IV that the

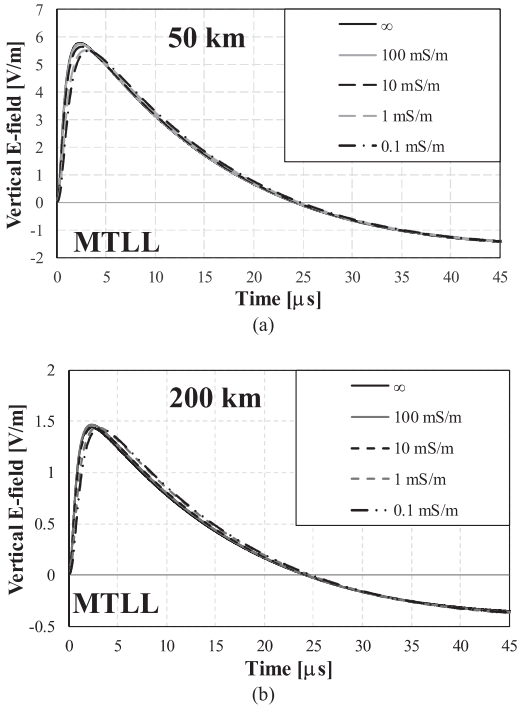

Fig. 6. Waveforms of E_z at distances of (a) $r = 50$ km and (b) $r = 200$ km from the lightning channel, computed using the FDTD method with the MTLL model for different values of ground conductivity: $\sigma = 0.1$, 1, 10, and 100 mS/m compensated for propagation effects using (10). Waveforms computed for $\sigma = \infty$ are also shown for reference. $RT = 1$ μs.

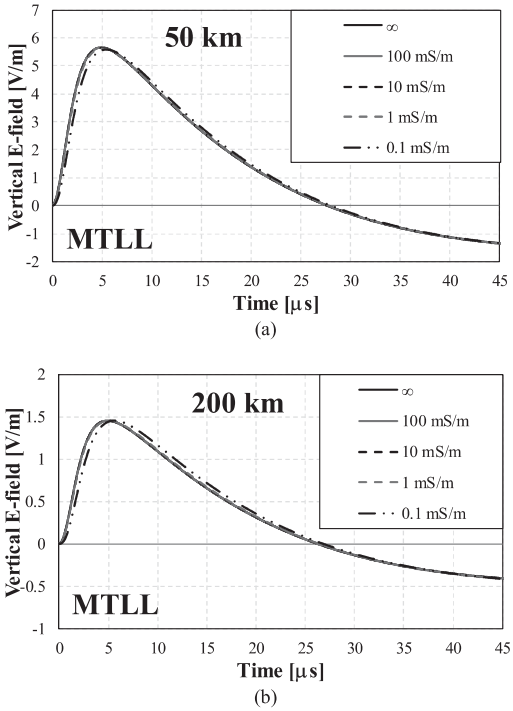

Fig. 7. Same as Fig. 6, but for $RT = 5$ μs.

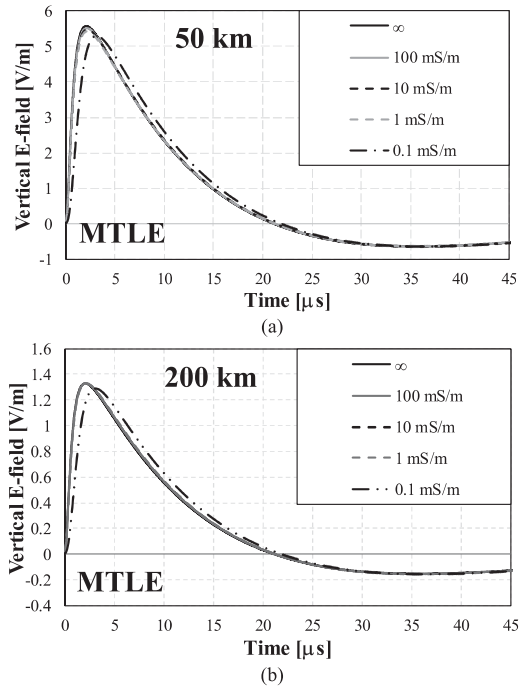

Fig. 8. Same as Fig. 6, but for the MTLE model.

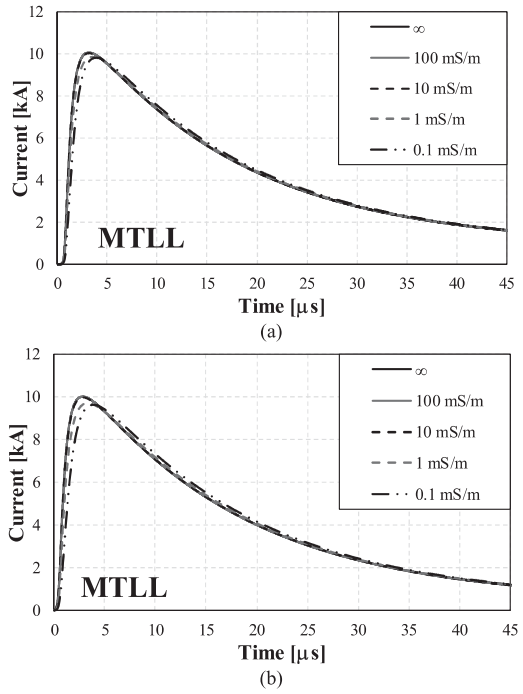

Fig. 9. Waveforms of lightning return-stroke current at the channel base reconstructed, using (5), from electric-field waveforms (a) at 50 km and (b) at 200 km compensated for propagation effects and shown in Fig. 6.

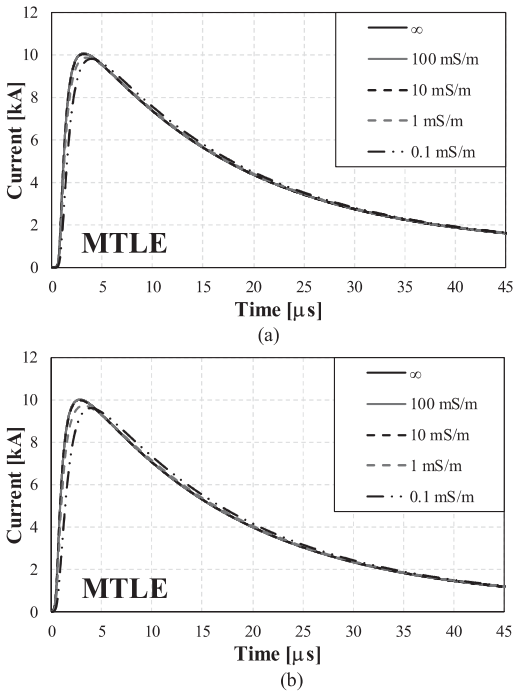

Fig. 10. Same as Fig. 9, but for the MTLE model.

TABLE II
SAME AS TABLE I, BUT FOR $RT = 5$ μS

Distance	Ground conductivity σ, mS/m			
r, km	0.1	1	10	100
50	9.92	9.93	9.97	9.98
100	9.89	9.92	9.97	9.98
200	9.87	9.90	9.95	9.97

TABLE III
PEAK VALUES OF ESTIMATED CHANNEL-BASE CURRENT IN KA FOR THE MTLE MODEL AND $RT = 1$ μS

Distance	Ground conductivity σ, mS/m			
r, km	0.1	1	10	100
50	9.89	9.92	9.95	9.98
100	9.85	9.87	9.95	9.98
200	9.81	9.84	9.94	9.97

TABLE IV
SAME AS TABLE III, BUT FOR $RT = 5$ μS

Distance	Ground conductivity σ, mS/m			
r, km	0.1	1	10	100
50	9.91	9.95	9.97	9.98
100	9.88	9.95	9.97	9.98
200	9.87	9.94	9.96	9.97

reconstructed peak values of the channel-base current are in excellent agreement with the actual peak current value (10 kA).

The current reconstruction results presented earlier are not significantly influenced by the return-stroke model (MTLL or MTLE), current risetime (1 or 5 μs), distance (50–200 km), or

(ground) conductivity (0.1–100 mS/m). The potential influence of the uncertainty in the return-stroke speed (when it is not available from optical observation) will be examined in a future study.

VI. Summary

First, expressions for reconstructing the channel-base current waveform from E_z waveform on perfectly conducting ground have been proposed for the MTLL and MTLE return-stroke models. Second, E_z waveforms on lossy ground have been computed at far distances using the FDTD method for the same two models. Third, the FDTD-computed E_z waveforms on lossy ground have been compensated for propagation effects using the procedure proposed in [6]. Finally, channel-base current waveforms have been inferred from the compensated E_z waveforms using the proposed field-to-current conversion expressions. The reconstructed current waveforms are in excellent agreement with the current waveform that was used in computing E_z on lossy ground.

References

[1] V. A. Rakov, *Fundamentals of Lightning*. Cambridge Univ. Press: U.K., 2016, pp. 99–102.
[2] M. Popov, S. He, and R. Thottappillil, "Reconstruction of lightning currents and return stroke model parameters using remote electromagnetic fields," *J. Geophys. Res.*, vol. 105, no. D19, pp. 24469–24481, Oct. 2000.
[3] V. A. Rakov and A. A. Dulzon, "Calculated electromagnetic fields of lightning return stroke," *Tekhnicheskaya Elektrodinamika*, vol. 1, pp. 87–89, 1987.
[4] C. A. Nucci, C. Mazzetti, F. rachidi, and M. Ianoz, "On lightning return stroke models for LEMP calculation," in *Proc. Paper presented at 19th Int. Conf. Lightning Protection*, 1988, pp. 463–470.
[5] K. S. Yee, "Numerical solution of initial boundary value problems involving Maxwell's equations in isotropic media," *IEEE Trans. Antennas Propag.*, vol. 14, no. 3, pp. 302–307, May 1966.
[6] V. Cooray, "Effects of propagation on the return stroke radiation fields," *Radio Sci.*, vol. 22, no. 2, pp. 757–768, Sep./Oct. 1987.
[7] M. Fukuyama, S. Koike, Y. Baba, T. Tsuboi, and V. A. Rakov, "Reconstruction of channel base current waveforms from electromagnetic field waveforms degraded by propagation effects," paper presented at 35th Int. Conf. Lightning Protection XVI Int. Symp. Lightning Protection, 2021, p. 7.
[8] F. Rachidi and R. Thottappillil, "Determination of lightning currents from far electromagnetic fields," *J. Geophys. Res.*, vol. 98, no. D10, pp. 18 315–18 321, Oct. 1993.
[9] Z. P. Liao, H. L. Wong, B. P. Yung, and Y. F. Yuan, "A transmitting boundary for transient wave analysis," *Sci. China*, vol. 27, no. 10, pp. 1063–1076, 1984.
[10] Y. Baba and V. A. Rakov, "On the transmission line model for lightning return stroke representation," *Geophys. Res. Lett.*, vol. 30, no. 24, p. 4, Dec. 2003, doi: 10.1029/2003GL018407.
[11] F. Heidler, "Traveling current source model for LEMP calculation," in *Proc. Int. Symp. Electromagn. Compat.*, 1985, pp. 157–162.

Shunsuke Koike received the B.Ss. and M.Sc. degrees in electrical engineering from Doshisha University, Kyoto, Japan, in 2021 and 2023, respectively.

His research interest includes computational electromagnetics.

Masahiro Fukuyama received the B.Ss. and M.Sc. degrees in electrical engineering from Doshisha University, Kyoto, Japan, in 2019 and 2021, respectively.

His research interest includes computational electromagnetics.

Yoshihiro Baba (Fellow, IEEE) received the B.Sc., M.Sc., and Ph.D. degrees in electrical engineering from the University of Tokyo, Tokyo, Japan, in 1994, 1996, and 1999, respectively.

Since 2012, he has been a Professor with Doshisha University, Kyoto, Japan, and the Dean of the Institute of Advanced Research and Education since 2022. From 2003 to 2004, he was a Visiting Scholar with the University of Florida, Gainesville, FL, USA. He is the author or coauthor of 4 books, 7 book chapters, and more than 130 papers published in reviewed international journals.

Dr. Baba was the recipient of the Technical Achievement Award from the IEEE EMC Society in 2014. He was an Editor for IEEE Transactions on Power Delivery from 2009 to 2018, a Guest Associate Editor for IEEE Transactions on Electromagnetic Compatibility from 2018 to 2019, and an Associate Editor for *Electrical Engineering* (Springer Journal) from 2019 to 2022. He was the Convener of C4.37 Working Group of the International Council on Large Electric Systems from 2014 to 2019, and a Vice President of the Power and Energy Society of the Institute of Electrical Engineers of Japan (IEEJ) from 2020 to 2022. He has been the Vice Chairperson of the Steering Committee of the Asia-Pacific International Conference on Lightning since 2017, and an Associate Editor for IEEE Transactions on Electromagnetic Compatibility since 2022. He is a Fellow of the Institution of Engineering and Technology and the IEEJ.

Toshihiro Tsuboi received the B.Sc. and M.Sc. degrees in electrical engineering from the Tokyo Institute of Technology, Tokyo, Japan, in 1997 and 1999, respectively, and the Ph.D. degree in electrical engineering from Chiba University, Chiba, Japan, in 2013.

In 1999, he joined Tokyo Electric Power Company Research Institute, Yokohama, Japan, where he is currently a Senior Researcher. Since 2020, he has been an Adjunct Professor with Doshisha University, Kyoto, Japan. His main research interest includes insulation design of power systems.

Vladimir A. Rakov (Fellow, IEEE) received the M.S. and Ph.D. degrees in electrical engineering from Tomsk Polytechnical University (Tomsk Polytechnic), Tomsk, Russia, in 1977 and 1983, respectively.

From 1977 to 1979, he was an Assistant Professor of Electrical Engineering, Tomsk Polytechnic. In 1978, he joined the Lightning Research Group, High Voltage Research Institute (a division of Tomsk Polytechnic), where from 1984 to 1994, he held the position of the Director of the Lightning Research Laboratory. He is currently a Distinguished Professor with the Department of Electrical and Computer Engineering, University of Florida, Gainesville, FL, USA, and the Director of the International Center for Lightning Research and Testing (ICLRT). He is the author or coauthor of 5 books, and more than 800 other publications on various aspects of lightning, with more than 300 papers being published in reviewed journals.

Dr. Rakov is a Fellow of the American Geophysical Union, the American Meteorological Society, and the Institution of Engineering and Technology.